8944 *Biochemistry* **2010,** *49,* 8944–8954
DOI: 10.1021/bi1008062

BIOCHEMISTRY
including biophysical chemistry & molecular biology
Article

ADP-Ribosylation of Cross-Linked Actin Generates Barbed-End Polymerization-Deficient F-Actin Oligomers[†]

Alexandru A. Perieteanu, Danielle D. Visschedyk, A. Rod Merrill, and John F. Dawson*

University of Guelph, Guelph, Ontario, Canada N1G 2W1

Received May 20, 2010; Revised Manuscript Received August 21, 2010

ABSTRACT: Actin filament subunit interfaces are required for the proper interaction between filamentous actin (F-actin) and actin binding proteins (ABPs). The production of small F-actin complexes mimicking such interfaces would be a significant advance toward understanding the atomic interactions between F-actin and its many binding partners. We produced actin lateral dimers and trimers derived from F-actin and rendered polymerization-deficient by ADP-ribosylation of Arg-177. The degree of modification resulted in a moderate reduction in thermal stability. Calculated hydrodynamic radii were comparable to theoretical values derived from recent models of F-actin. Filament capping capabilities were retained and yielded pointed-end dissociation constants similar those of wild-type actin, suggesting native or near-native interfaces on the oligomers. Changes in DNase I binding affinity under low and high ionic strength suggested a high degree of conformational flexibility in the dimer and trimer. Polymer nucleation activity was lost upon ADP-ribosylation and rescued upon enzyme-mediated deADP-ribosylation, or upon binding to gelsolin, suggesting that interactions with actin binding proteins can overcome the inhibiting activities of ADP-ribosylation. The combined strategy of chemical cross-linking and ADP-ribosylation provides a minimalistic and reversible approach to engineering polymerization-deficient F-actin oligomers that are able to act as F-actin binding protein scaffolds.

Actin is a eukaryotic protein that is essential for a myriad of biochemical processes such as cellular mobility, cytokinesis, sarcomere contraction, and protein transport (*32*, *36*). Under physiological conditions, globular actin (G-actin) self-associates to form long double-stranded, right-handed helical actin filaments (F-actin) containing hundreds of actin subunits. In the cell, an array of actin binding proteins (ABPs)[1] control and/or take advantage of actin polymerization (*5*). Two general classes of F-actin-specific ABPs exist: those that bind to the ends of filaments (capping proteins) and those that bind along the length of the filaments (side-binding ABPs). In actin filaments, adjacent actin subunits are responsible for the formation of these critical ABP binding interfaces.

The goal of this research is to develop short F-actin oligomers to serve as structural platforms for the elucidation of molecular interactions between F-actin and ABPs. Any strategy to this end involves two aspects: (1) covalent cross-linking of actin subunits in F-actin and (2) modification of the resulting actin oligomers to inhibit actin polymerization. The extent of these modifications must be strategically balanced with maintaining physiological interactions that are integral to F-actin function.

Previous work has shown that an actin longitudinal (or long-pitch) dimer can be formed by covalently cross-linking Gln-41 to Cys-374 of adjacent protomers using *N*-(4-azido-2-nitrophenyl)putresceine (ANP) (*11*). ANP-actin dimers were also shown to maintain some affinity for the N-terminal segment of gelsolin, deoxyribonuclease I (DNase I), and myosin subfragment 1 (*22*). Conversely, lateral (or short-pitch) actin dimers have been produced by covalently cross-linking Cys-374 to Lys-191 of adjacent protomers using *N*,*N*′-*p*-phenylenebismaleimide (PBM) (*18*, *25*, *34*). Similarly, PBM trimers possessing both lateral and longitudinal contacts have been constructed and shown to act as filament nuclei, essentially increasing filament growth kinetics by circumventing slow nucleation events (*8*, *18*).

Three general modification strategies have been used to inhibit actin polymerization: translational modifications (*14*, *29*, *41*), covalent posttranslational modifications (*9*, *17*, *19*), and noncovalent posttranslational modifications (*2*, *4*, *16*, *23*, *27*). Here, we employ a recently discovered mono-ADP-ribosyltransferase from *Photorhabdus luminescens* to specifically modify PBM-cross-linked actin oligomers (*39*). ADP-ribosyltransferase enzymes (ADPRTs) covalently transfer an ADP-ribose (ADPr) moiety from NAD^+ to a target protein. ADP-ribosylation at Arg-177 of actin is also catalyzed by a variety of other, classical ADPRTs such as *Clostridium perfringens* iota toxin, *Clostridium botulinum* C2 toxin, and *Salmonella enterica* virulence protein SpvB.

In this work we use a combined strategy of PBM cross-linking and ADP-ribosylation to produce and purify polymerization-deficient short-pitch actin dimers (ADPr dimer) and actin trimers (ADPr trimer). Both ADPr dimer and ADPr trimer were found to possess similar hydrodynamic radii to those calculated from structural data, suggesting that both species adopt a physiological conformation. While the modifications result in slightly decreased thermal stability and altered nucleotide exchange kinetics, the constructs possessed conformational flexibility and retained their ability to cap existing filament barbed ends. Finally, we found that the filament nucleation capabilities of actin dimers and trimers were abolished upon ADP-ribosylation

[†]This work was supported by NSERC Grant 250188-04 to J.F.D. and grants from HSFP, CIHR, and CCF to A.R.M.

*Address correspondence to this author. Tel: (519) 824-4120 ext 58181. Fax: (519) 837-1802. E-mail: jdawso01@uoguelph.ca.

[1]Abbreviations: PBM, *N*,*N*′-*p*-phenylenebismaleimide; ADPr, ADP-ribosylated; [NBD], concentration based on nucleotide binding domains; β-ME, 2-mercaptoethanol; DNase I, deoxyribonuclease I; ABPs, actin binding proteins; py-actin, pyrene iodoacetamide labeled actin; ADPr-py-actin, ADP-ribosylated py-actin; C_c, critical concentration; MWCO, molecular weight cutoff.

 Published on Web 08/26/2010

but were rescued upon enzyme-mediated reversal of the ADP-ribosylation (deADPr) and upon structural remodeling induced by gelsolin binding. This study provides a minimalistic and reversible approach to engineering polymerization-deficient F-actin oligomers able to act as F-actin binding protein scaffolds.

EXPERIMENTAL PROCEDURES

Reagents. All reagents were purchased from either Sigma-Aldrich (St. Louis, MO) or Fisher Scientific (Mississauga, Ontario, Canada). Chromatographic columns were supplied by GE Healthcare (Piscataway, NJ). Purifications were performed on an AKTA FPLC system. Protein concentrators (10 kDa MWCO) were purchased from Millipore (Billerica, MA).

Protein Preparation. Skeletal muscle acetone powder was prepared from chicken breast as described by Spudich and Watt (*37*). Actin concentrations were determined from absorbance at 290 nm using an extinction coefficient of 67742 M^{-1} cm^{-1} or using the Bio-Rad protein assay (Mississauga, Ontario, Canada). Actin samples in G-buffer (2 mM Tris-HCl, 0.2 mM $CaCl_2$, 0.2 mM ATP, 0.2 mM 2-mercaptoethanol, β-ME) were frozen in liquid N_2 and stored at −70 °C unless used for cross-linking. Where applicable, we report concentrations based on the presence of high-affinity nucleotide binding domains [NBD], allowing for differentiation between actin subunit concentration and the concentration of total complex.

Photox was purified from insoluble inclusion bodies as previously described (*39*). The resulting protein was dialyzed into 20 mM Tris-HCl, pH 7.5, and 50 mM NaCl, concentrated to 0.2−1.0 mg/mL, and stored at −70 °C.

Human gelsolin was prepared as described (*26*) and stored at −70 °C. ADPr trimer−gelsolin heterocomplexes were formed by incubating 1:1 ADPr trimer and gelsolin, followed by purification on a Superdex S200 column preequilibrated in buffer G-10 (10 mM Tris-HCl, pH 8.0, 0.2 mM $CaCl_2$, 0.2 mM ATP, 0.2 mM β-ME, 0.2 mM NaN_3, 0.25 mM phenylmethanesulfonyl fluoride) with 50 mM NaCl. Purity and composition were assessed by native PAGE and SDS−PAGE (data not shown).

Bovine pancreas deoxyribonuclease I (DNase I) purchased from Worthington Biochemical Corp. (Lakewood, NJ) was purified using a Superdex S200 gel chromatography column to remove traces of a higher molecular weight impurity (data not shown). Samples were flash frozen in liquid N_2 and stored at −70 °C. Gelsolin and DNase I were thawed and exchanged into G-buffer using HiTrap desalting columns for native PAGE binding assays. Bio-Rad protein assay was employed for concentration determination of gelsolin and DNase I.

ADP-Ribosylation and De-ADP-ribosylation. Actin samples were diluted to 25−100 μM and the G-buffer Tris-HCl, pH 8.0, concentration was increased to 10 mM. Samples were incubated with 20−200 nM photox (0.1−1% v/v), and a 5−10-fold molar excess of NAD^+ was titrated into the sample mixture with slow stirring over a period of 15 min. Enzymatic activity was monitored upon addition of toxin using fluorescence (excitation 305 nm, emission 405 nm) and the NAD^+ analogue, etheno-NAD^+ (ε-NAD^+).

ADPr-actin samples were exchanged into 20 mM 2-(*N*-morpholino)ethanesulfonic acid, pH 6.5, G-buffer supplemented with 30 nM nicotinamide. ADP-ribosylation reversal was initiated by the addition of 200 nM photox and allowed to proceed overnight at 4 °C while being dialyzed against 30 nM nicotinamide. Samples were then exchanged into G-buffer.

Actin Cross-Linking with PBM. Chemical cross-linking of actin with PBM was performed as described (*18*) with some modifications. Actin (3−6 mg/mL) was polymerized at pH 8.0 by the addition of 50 mM KCl and 2 mM $MgCl_2$ under ambient temperature for 1−3 h. Cross-linking of actin was initiated by the addition of 10 mM sodium tetraborate, pH 9.0, and a 1.5-fold molar excess of a 25 mM stock solution of PBM dissolved in DMF and terminated after 30 min at ambient temperature using a 150-fold molar excess of β-ME over PBM. Cross-linked F-actin was harvested by centrifugation at 167424*g* for 75 min and resuspended in G-buffer to a final concentration of 1−2 mg/mL. The resulting PBM-cross-linked actin mixture was dialyzed extensively over 3−4 days with at least five buffer exchanges to depolymerize cross-linked filaments. ADP-ribosylation was initiated as described above. Remaining F-actin was removed by centrifugation at 167424*g* for 75 min. Samples were concentrated and applied to a Superdex S200 column preequilibrated in buffer G-10 with 50 mM NaCl. Fractions containing ADPr dimer and ADPr trimer were pooled, and iterations of gel filtration were performed. As a final measure, polymerization was induced over a period of 30 min, and samples were centrifuged at 392000*g* for 20 min. Supernatants (2−7 mg/mL) were then dialyzed against buffer G-10, flash frozen in liquid N_2, and stored at −70 °C. When utilized, samples were desalted into G-buffer and used within 2 days of thawing.

Polymerization. Polymerization was monitored using three techniques.

(*1*) *Light Scattering Intensity Copolymerization*. Actin (0−20 μM) and ADP-ribosylated actin (0−20 μM) were brought to ambient temperature, and polymerization was induced with a 10-fold stock solution of polymerization salts (250 mM Tris-HCl, pH 8.0, 500 mM KCl, 20 mM $MgCl_2$, 2 mM ATP, and 10 mM EGTA), yielding F-buffer. Light scattering at 90° to the incident light beam was monitored using a pulsed-beam Varian Cary Eclipse fluorescence spectrophotometer (Mississauga, Ontario, Canada) at an excitation of 360 nm and emission of 360 nm. All solutions were passed through 0.22 μm filters to minimize background light scattering, and experiments were performed with a replicate number of $n \geq 3$.

(*2*) *Pyrene Polymerization Assay*. Skeletal actin was labeled with pyrene iodoacetamide (py-actin) as previously described (*3*). Actin samples in G-buffer were diluted and brought to 2.5% py-actin prior to induction of polymerization. Polymerization of 10 μM [NBD] of actin, ADPr-actin, ADPr dimer, or ADPr trimer was initiated by the addition of stock polymerization salts. Fluorescence intensity was monitored using a Cary Eclipse spectrofluorometer at excitation and emission wavelengths of 347 and 407 nm, respectively. Nucleation experiments were similarly performed in triplicate with 5 μM actin (2.5% py-actin) substituted with 0.25 μM [NBD] of the nuclei being examined.

Pyrene fluorescence was also used for monitoring the copolymerization of actin and pyrene-labeled ADPr-actin (ADPr-py-actin). Briefly, py-actin was ADP-ribosylated as described above and excess NAD^+ removed by gel-filtration chromatography. Samples containing 2 μM ADPr-py-actin and increasing concentrations of actin (0−50 μM) were monitored after the introduction of stock polymerization salts. Experiments were also performed using non-ADP-ribosylated py-actin. The ratios of the baseline-corrected steady-state (180 min) change in fluorescence (ΔF) intensities of ADPr-py-actin and py-actin were plotted against the concentration of unmodified actin; a curve representing the proportion of ADPr-py-actin filament incorporation was generated. Assembly curves generated using Sephadex S300 purified actin did not yield different results.

(*3*) *Polymerization Sedimentation Assay*. Polymerization of 20 μM [NBD] actin, ADPr-actin, ADPr dimer, or ADPr trimer was induced by incubating the samples in polymerization salts for 3 h at room temperature. Samples were subjected to centrifugation at 392000*g* for 20 min. Supernatants and pellets were separated and analyzed by SDS−PAGE.

Dual-Color Filament Capping Assay. The dual-color filament capping assay was performed as described by Harris et al. (*10*). Actin (4 μM) was polymerized for 4 h in F-buffer. Samples were diluted 2-fold with 300 nM ADPr-actin, dimer, or trimer and allowed to incubate at ambient temperature for 5 min. Samples were again diluted 2-fold with equimolar rhodamine-phalloidin. Samples were further diluted 10-fold with 400 nM G-actin and 400 nM Alexa 488-phalloidin and rapidly brought to F-buffer conditions using concentrated stock. The solution was allowed to incubate for 10 min before being diluted an additional 5-fold with F-buffer supplemented with 3 mg/mL glucose, 120 μg/mL glucose oxidase, and 18 μg/mL catalase. The final mixture (1 μL) was loaded onto a 0.01% poly-(L-lysine)-coated slide. Images were taken through rhodamine and fluorescein filters. The percent occurrence of two colored events was determined and plotted for each condition. At least six images were analyzed, totaling at least 300 independent filaments for each sample. The standard deviation of the mean percent occurrence was calculated from the variance between images.

Inhibition of Actin Nucleation Assay. Polymerization of actin in the presence of filament nuclei was monitored using an Applied Photophysics SX20 stopped-flow spectrofluorometer (Surrey, U.K.) set to an excitation wavelength of 350 nm and an emission cutoff filter of 395 nm. F-Actin (1 μM, 5% py-actin) in 5 mM Tris-HCl, pH 8.0, 4 mM $MgCl_2$, 100 mM KCl, 0.2 mM ATP, and 0.2 mM β-ME was mixed with 1 volume of 3 μM actin and 5% py-actin in 5 mM Tris-HCl, pH 8.0, 0.2 mM $CaCl_2$, 0.2 mM ATP, and 0.2 mM β-ME supplemented with 0.002−2.0 μM ADPr-actin, ADPr dimer, or ADPr trimer. The rate of polymerization between 25 and 50 s was plotted against the concentration of ADP-ribosylated actin, and a binding isotherm was used to extrapolate the apparent dissociation constants (K_d^{app}) for ADPr-actin and its oligomers to the barbed end of actin filaments. Assembly curves generated using Sephadex S300 purified actin did not yield different results.

Acrylamide Gel Electrophoresis. SDS−PAGE was performed as described previously (*20*) and visualized by staining with Coomassie Brilliant Blue R250 or under UV light. Native PAGE was performed with 8% nonreducing, nondenaturing acrylamide gels supplemented with 0.2 mM ATP and 0.2 mM $CaCl_2$. Native PAGE electrophoresis was also performed on ice at low voltage (< 80 V).

Dynamic Light Scattering. Actin and ADPr-actin were purified using Sephadex S300 gel filtration chromatography. Peak fractions corresponding to the latter half of the monomeric peak were pooled and filtered through a 0.22 μM filtration device. Concentrations were determined and adjusted to 0.25 mg/mL using filtered G-buffer. Similarly, column-purified ADPr dimer and ADPr trimer were thawed, diluted, and filtered. Dynamic light scattering measurements were performed on a Nano S Zetasizer (Malvern, U.K.) equipped with a 633 nm red laser and a 173° backscatter detector. A normal distribution fit of volume distribution measurements was used to determine the experimental Stokes radius of all samples. All radii were calculated from $n \geq 9$ distribution measurements. Theoretical radii were calculated using HydroPRO version 7c (*7*).

Thermal Unfolding. The transition temperatures for actin and the various complexes were determined using a JASCO-815 chiro-optical spectrometer equipped with a PTC-424S/15 Peltier temperature control unit. Actin protein species were dialyzed twice at 4 °C against their respective buffers. Actin protein species concentrations were adjusted to 0.16 mg/mL (3.8 μM [NBD]) using the appropriate buffer system. A scan rate of 1 °C/min was applied, and the absorbance at 222 nm was monitored through a 1 mm quartz cuvette. The transition temperature was defined as the minima of a Weibull fit to the first derivative of the unfolding profile as described (*30*). Transition temperatures were calculated from a minimum of three thermal scans.

Nucleotide Release. Purified polymerization-deficient actin complexes were buffer-exchanged into nucleotide-free G-buffer using a HiTrap desalting column (GE Healthcare, Piscataway, NJ). The protein-containing fractions were quickly pooled and supplemented with a final concentration of 0.2 mM ε-ATP. Samples were incubated for 3−5 h on ice, buffer exchanged into nucleotide-free G-buffer, and supplemented with 20 μM ε-ATP. Samples were incubated for a minimum of 30 min prior to fluorometric analysis. Protein concentrations were determined, and samples were diluted to 2 μM [NBD]. Sample measurements from three separate injections were recorded using an Applied Photophysics SX20 stopped-flow apparatus (Surrey, U.K.) with an excitation wavelength of 350 nm and an emission cutoff filter of 395 nm.

DNase I Inhibition. DNase I inhibition was performed as described (*26*). Activity measurements were performed with a replicate number $n \geq 3$.

RESULTS AND DISCUSSION

Actin−ADPr-Actin Copolymerization. ADP-ribosylated actin is known to copolymerize with unmodified actin, but a detailed analysis of the degree to which copolymerization occurs has not been conducted (*1*). We sought to test this as it would pose as a potential obstacle to the production of polymerization-deficient actin oligomers. ADP-ribosylated actin labeled with pyrene on Cys-374 (ADPr-py-actin) was used as a sensitive means to determine the extent of copolymerization. Polymerization of both py-actin and ADPr-py-actin (2 μM) was induced in the presence of increasing concentrations of unmodified actin (0−50 μM) and the maximum fluorescence recorded (Figure 1A). The ratio of maximum fluorescence intensities was plotted against unmodified actin concentration to show the relative proportion of ADPr-py-actin incorporation into the filaments (Figure 1B). For 2 μM ADPr-py-actin, we found a 50% efficiency of incorporation ($EI_{0.5}$) of 18 μM and an estimated $EI_{0.9}$ of 150 μM. Therefore, at a 9:1 ratio of unmodified actin to ADPr-py-actin, 50% of the available ADPr-actin was incorporated into actin filaments. Furthermore, > 90% incorporation was extrapolated to occur only at ratios of actin to ADPr-py-actin of > 75:1. An ADPr trimer modified with only one ADP-ribose would possess an actin to ADPr-actin ratio of 2:1 and, based on our data, would have an efficiency of incorporation < 18%. Substoichiometric ADP-ribosylation of cross-linked actin dimers and trimers could potentially retain a small degree of polymerizability, and therefore a cautionary approach to producing polymerization-deficient oligomers should be taken.

To gain an understanding of the effect that the presence of ADPr-actin has on the polymerization properties of actin, we used light scattering intensity (LSI) to monitor the salt-induced polymerization of 20 μM total actin with varying ratios

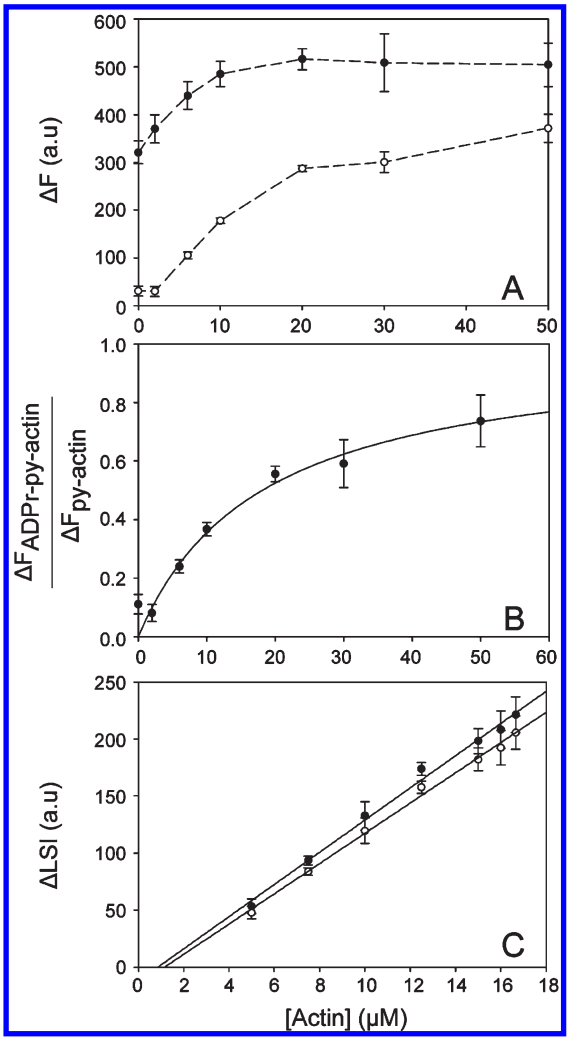

FIGURE 1: Copolymerization of actin and ADPr-actin. (A) The change in fluorescence intensity (ΔF) at steady state (180 min) after copolymerization of 2 μM py-actin (●) or ADPr-py-actin (○) with varying concentrations (0−50 μM) of unmodified skeletal actin. (B) The efficiency of filament incorporation of ADPr-py-actin plotted against the concentration of unmodified actin. $EI_{0.5}$ and $EI_{0.9}$ values of 18 and 150 μM, respectively, were determined. (C) The change in light scattering intensity, ΔLSI, after 200 min was plotted against unmodified actin (○) where actin concentrations ranged from 5.00 to 16.67 μM and samples were supplemented ADPr-actin to yield a total actin concentration of 20 μM. The ΔLSI attributable to unmodified actin was calculated by correcting for the contribution associated with ADPr-actin incorporation into filaments (●). The x-intercepts of linear regression represent apparent critical concentrations of 0.87 ± 0.44 and 1.16 μM for unaltered and corrected data, respectively.

of ADPr-actin to actin (Supporting Information Figure S1). Given our previous observations of copolymerization, we could assume that some of the light scattering was due to ADPr-actin being incorporated into actin filaments. Utilizing our copolymerization data from Figure 1B, we determined that only 7−11% of the LSI was attributable to ADPr-actin copolymerization. The change in LSI (ΔLSI) upon the addition of polymerization salts was plotted as a function of unmodified actin concentration, and an apparent critical concentration (C_c) of 0.87 ± 0.44 μM was determined from the x-intercept of the plot (Figure 1C). Furthermore, the corrected change in LSI attributable only to unmodified actin polymerization was also plotted, and a similar C_c of 1.16 μM was calculated. Previously reported C_c values for skeletal α-actin are 0.12 ± 0.07 and 0.60 ± 0.17 μM for the barbed and pointed ends, respectively (*31*). Since our calculated C_c values are similar to that of the pointed end of actin, it is likely that ADPr-actin caps actin filaments at their barbed ends, allowing them only to polymerize at the pointed end, a conclusion that has also been reached by other authors through different means (*40*).

Formation and Purification of ADP-Ribosylated PBM-Cross-Linked Actin Oligomer. Chemical cross-linking of actin with PBM was performed as described by Knight and Offer (*18*). Reaction conditions were reexamined with the intention of maximizing trimer yields (Supporting Information Figure S2). In short, slightly increased trimer yields were found with longer reaction times.

ADP-ribosylation of PBM-actin oligomers was detectable by UV visualization when using ε-NAD^+ as the transferase substrate (Figure 2A, inset) indicating successful ADP-ribosylation of PBM-actin dimers and trimers, as well as higher order oligomers. Using ε-NAD^+ as a substrate, we were also able to monitor the enzymatic reaction in real time (Figure 2A). Under the conditions tested, ADP-ribosylation reactions were largely completed within 30 min; however, since it is not uncommon for cross-linked actin filaments to remain partially oligomeric, longer reaction times were employed to allow for ADP-ribosylation of treadmilling filaments. Successive gel filtration chromatography steps were performed to separate discrete oligomeric species (Figure 2B). While the procedure was labor-intensive, it was reproducible, and the chromatographic steps could be automated using the computer-driven AKTA FPLC system. SDS−PAGE analysis of the progress of purification is shown in Figure 2C. ADPr dimer and ADPr trimer yields at critical stages of the purification process are summarized in Supporting Information Table S1.

The two-step strategy employing PBM cross-linking and ADP-ribosylation to produce and purify actin dimers and trimers yielded milligram quantities of highly pure actin dimers and trimers. An assessment of the impact of the introduced modifications on the biochemical/biophysical properties of both ADPr dimer and ADPr trimer was conducted prior to using them as an ABP scaffold.

PBM and ADP-Ribose Stoichiometry. The copolymerization data presented above suggest that the degree to which actin dimers and trimers are ADP-ribosylated could play a role in rendering these oligomers polymerization-deficient. The extent to which the actin oligomers were modified was determined by mass spectrometry (data not shown). A 1:1 ADP-ribose to actin stoichiometry was detected for both the ADPr dimer and ADPr trimer. Thus, it appears that photox is able to ADP-ribosylate each subunit in the complex, irrespective of steric constraints introduced by chemical cross-linking. Since at least one Arg-177 is expected to be blocked in an F-actin conformation, the data suggest that, under low ionic strength, PBM dimers and trimers are conformationally flexible. Stoichiometric ADP-ribosylation may result in the disruption of intermolecular contacts; however, it does provide two key advantages over substoichiometric ADP-ribosylation: (1) substoichiometric labeling may result in the retention of some polymerization especially in the case of the actin trimer, whereas this is not a concern when the oligomers are fully modified, and (2) stoichiometric modification of the oligomers eliminates concerns about the heterogeneity of the modification. Furthermore, the presence of a cross-linking moiety may introduce enough covalent constraint to overcome any major perturbations introduced by the ADP-ribose.

The extent of PBM cross-linking was also determined using mass spectrometry. ADPr dimer showed an equal mixture of

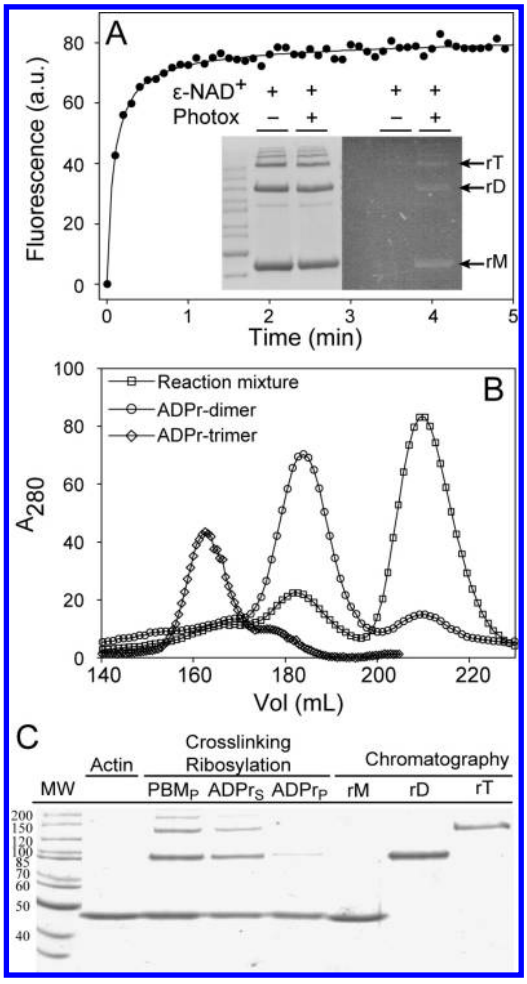

FIGURE 2: ADP-ribosylation and purification of PBM cross-linked skeletal actin. (A) Fluorescence intensity time course measurement of ADP-ribosylation of a 1.5 mg/mL PBM−actin mixture in the presence of 180 μM ε-NAD$^+$ and 200 nM photox. SDS−PAGE of PBM cross-linked actin (1.5 mg/mL) in 10 mM Tris-HCl and 180 μM ε-NAD$^+$ G-buffer in the absence or presence of 200 nM photox. In the presence of photox, UV visualization showed ADP-ribosylation of all actin species (inset). Arrows indicate ADP-ribosylated actin monomer (rM), dimer (rD), and trimer (rT) species. ADPr-actin and its oligomers. (B) Chromatographic purification of the reaction mixture (□), ADPr dimer (○), and ADPr trimer (◇) over a HiLoad 26/60 Superdex 200 gel filtration column. (C) SDS−PAGE of fractions retrieved from the purification process. PBM_P shows pelleted polymerization-competent actin proteins after cross-linking with PBM. $ADPr_S$ and $ADPr_P$ are supernatant and pellet fractions after photox treatment, with induction of polymerization prior to sedimentation. rM, rD, and rT represent purified ADPr monomer, dimer, and trimer.

actin dimers containing either one or two reacted PBM molecules, while ~25% of ADPr trimers contained two reacted PBM molecules, and 75% contained three reacted PBM molecules. In both cases, the additional cross-link is likely present on the available Cys-374 of the barbed-end actin subunit.

Dynamic Light Scattering. To ascertain the structural state of the ADPr-actin complexes, dynamic light scattering measurements were acquired for actin, ADPr-actin, its dimer, and its trimer (Figure 3). The measured hydrodynamic radii were compared with literature values and theoretical values from X-ray crystal structure data (Table 1, Supporting Information Figure S3). The results for actin and ADPr-actin are in agreement with previously determined values and theoretical values for monomeric actin (*7*, *9*, *28*). Likewise, the measured hydrodynamic

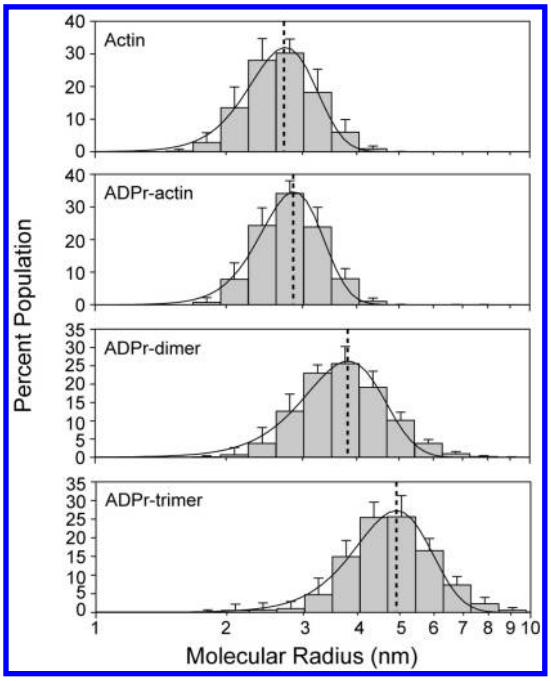

FIGURE 3: Dynamic light scattering measurements show ADP-ribosylated actin oligomers adopt F-actin conformations. Dynamic light scattering was performed on 0.25 mg/mL (A) actin, (B) ADPr-actin, (C) ADPr dimer, and (D) ADPr trimer. No significant increase in M_r was observed upon ADP-ribosylation of actin. An increase in M_r of 38% and 77% was detected for the ADPr dimer and ADPr trimer, respectively.

radius of 3.78 ± 0.22 nm for ADPr dimer agreed with theoretical values based on structural data and filament models (*34*). In contrast, a measured radius of 4.84 ± 0.41 nm for the ADPr trimer differs slightly from that of 4.52 nm calculated for a trimer from the Oda filament model, suggesting that, under monomer promoting conditions, the ADPr trimer is in a slightly more open conformation, perhaps due to the presence of an internal ADP-ribose.

Thermal Stability and Nucleotide Binding Affinity. Because of the significant amount of modification, we assessed the effect of cross-linking and ADP-ribosylation on the stability of the actin species produced by monitoring for the loss of secondary structure in the presence of a thermal gradient (Figure 4A). ADP-ribosylation alone reduced the transition temperature (T_m) of the monomer by 2.7 °C. Both ADPr dimer and trimer possessed similar thermal stabilities, about 3.5 °C lower than ADPr-actin and 5.2 °C lower than unmodified actin, indicating that both cross-linking and ADP-ribosylation are responsible for a decrease in thermal stability. Transition temperatures ranging from 52 to 59 °C are within the range of those tested for unmodified actin under various physiologically relevant conditions, indicating that the combined strategy of PBM cross-linking and ADP-ribosylation does not significantly destabilize the secondary structure of the oligomeric actin subunits (*30*, *35*).

The magnitude of the decrease in T_m between actin and the ADPr dimer or ADPr trimer was larger than that attributable to ADP-ribosylation alone, implying that either the cross-linker or another actin molecule in close proximity acted to destabilize the protein.

Current models suggest that actin unfolding is correlated with the loss of bound nucleotide (*30*). The dissociation of ε-ATP from actin was monitored in the presence of excess ATP (Figure 4B),

Table 1: Summary of Experimentally and Structurally Determined Biophysical Properties of Actin, ADPr-Actin, and Its Oligomers[a]

	molecular radii			binding terms				thermal stability and nucleotide exchange	
species	DLS M_r (nm)	M_r[c] (nm)	PDB	K_d^{app} (μM)	ΔG_f (eu)	ΔG_s (eu)	ΔS_r (eu/k)	T_m (°C)	$k_{\varepsilon\text{-ATP}}$ ($\times 10^{-3}$, s^{-1})
actin	2.73 ± 0.16	2.93	1NWK	0.121[b]	−9.27[c]	10.88[c]	−26.52[c]	58.7 ± 0.4	2.0 ± 0.1
		2.99	2ZWH					64.2 ± 0.7[d]	
ADPr-actin	2.86 ± 0.12	2.86	2GWJ	0.129 ± 0.031	−9.24	10.96	−26.80	56.0 ± 0.1	5.4 ± 0.7
ADPr dimer	3.78 ± 0.22	3.85	2Q36	0.030 ± 0.005	−10.08	11.45	−28.46	52.6 ± 0.1	6.1 ± 0.3
		3.92	2ZWH						
ADPr trimer	4.84 ± 0.41	4.52	2ZWH	0.072 ± 0.016	−9.57	11.88	−29.93	52.3 ± 0.6	5.5 ± 0.2

[a]The PDB accession numbers for the structural database used in the calculations are reported. Apparent dissociation constants determined by the competitive nucleation assay are summarized, and the binding energy terms determined using M_r and K_d^{app} data sets are reported. Thermal stability and nucleotide exchange parameters are also reported. [b]Values acquired and/or calculated from ref *31*. [c]Theoretical values calculated from PDB: 1NWK (*9*), 2ZWH (*28*), 2GWJ (*23*), and 2Q36 (*34*). [d]Transition temperature for actin under polymer-inducing conditions.

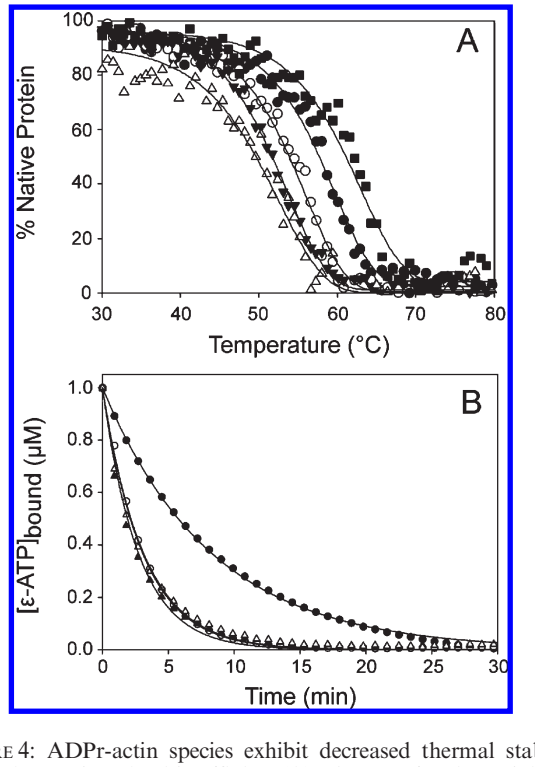

FIGURE 4: ADPr-actin species exhibit decreased thermal stability due to lowered nucleotide affinity. (A) The T_m of actin and ADP-ribosylated actin species was determined using circular dichroism. Representative isotherms for individual samples are shown. The T_m for monomeric actin under these conditions was found to be 58.7 ± 0.4 °C (●). Under similar conditions, a decrease of approximately 2.7 °C was observed with ADPr-actin (○). A 6.1 and 6.4 °C decrease was seen for ADPr dimer (▲) and ADPr trimer (Δ), respectively, compared to unmodified actin, and a 3.4 and 3.7 °C decrease in T_m when compared to ADPr-actin. Actin under polymerizing conditions is also shown (■). (B) Nucleotide exchange of ε-ATP-bound actin species. Actin species are represented by symbols as described above.

and apparent dissociation rates ($k_{\varepsilon\text{-ATP}}$) were calculated (summarized in Table 1). The increased rate of ε-ATP dissociation suggests that the presence of ADP-ribose at Arg-177 destabilized actin by a mechanism involving decreased nucleotide affinity. These results stress the importance of the relationship between nucleotide binding affinity and actin stability and that careful consideration should be taken when engineering these types of oligomers.

Polymerization of PBM-Cross-Linked ADPr-Actin Oligomers. Polymerization of ADPr-actin and its dimer and trimer was assessed using both pyrene-actin fluorescence and sedimentation analysis. No distinguishable increase in pyrene fluorescence characteristic of actin polymerization was observed upon addition of polymerization salts to ADPr-actin, dimer, or trimer (Supporting Information Figure S4). Sedimentation assays were performed to rule out the possibility that the pyrene fluorescence results were an artifact due to a deficiency in the interaction between pyrene-actin and ADPr-actin (Figure 5A). Under polymerizing conditions, unmodified actin readily sedimented and ADPr-modified actin and ADPr-actin oligomers remained in the supernatant, demonstrating that the ADP-ribosylation renders actin monomer, dimer, and trimer polymerization-deficient. The purification process includes polymerization/depolymerization cycles as well as chromatographic steps under conditions that favor polymerization. As a result, the purification conditions favor the purification of polymerization-deficient actin complexes. The purified products possessed a 1:1 ADP-ribose to actin stoichiometry and were subsequently shown to be polymerization-deficient. Copolymerization data suggest that substoichiometrically modified actin dimers and trimers may retain some degree of polymerization competency, and it is likely that substiochiometric ADP-ribosylation was not detected because the purification process selected against it.

ADPr-Actin Oligomers Cap Actin Filaments. Apparent C_c values attained from copolymerization experiments (Figure 1C) suggested that ADPr-actin retained the ability to bind the barbed end of actin filaments, essentially capping barbed ends and increasing the apparent C_c to a value equal to that of K_d at the pointed end. Having shown that ADPr dimer and ADPr trimer lack the ability to polymerize, it was of interest to determine whether the capping activity seen with ADPr-actin was retained, as it would imply the presence of an intact pointed-end surface.

Dual-color microscopy was performed in a manner similar to that described previously (*10*). Rhodamine-phalloidin stabilized filaments were doped with a low concentration (0.4 μM) of actin to minimize pointed-end elongation (Figure 5B). Actin elongating from the barbed end of rhodamine-phalloidin actin filaments (red) was stabilized by Alexa 488-phalloidin (green). In the absence of ADP-ribosylated actins, 42 ± 8% of the filaments were dual colored, suggesting that actin polymerized from the barbed end of these preformed rhodamine-phalloidin-bound actin filaments. In the presence of ADPr-actin, ADPr dimer, and ADPr trimer, the percent composition of dual-colored filaments decreased by approximately 75% to 14 ± 4%, 12 ± 4%, and 13 ± 5%, respectively (Figure 5C). These results suggest that the ADP-ribosylated actin species act as barbed-end cappers.

Binding of ADPr-actin and its dimer and trimer to F-actin was measured using a competitive nucleation assay (Supporting Information Figure S5). We found that the injection process on

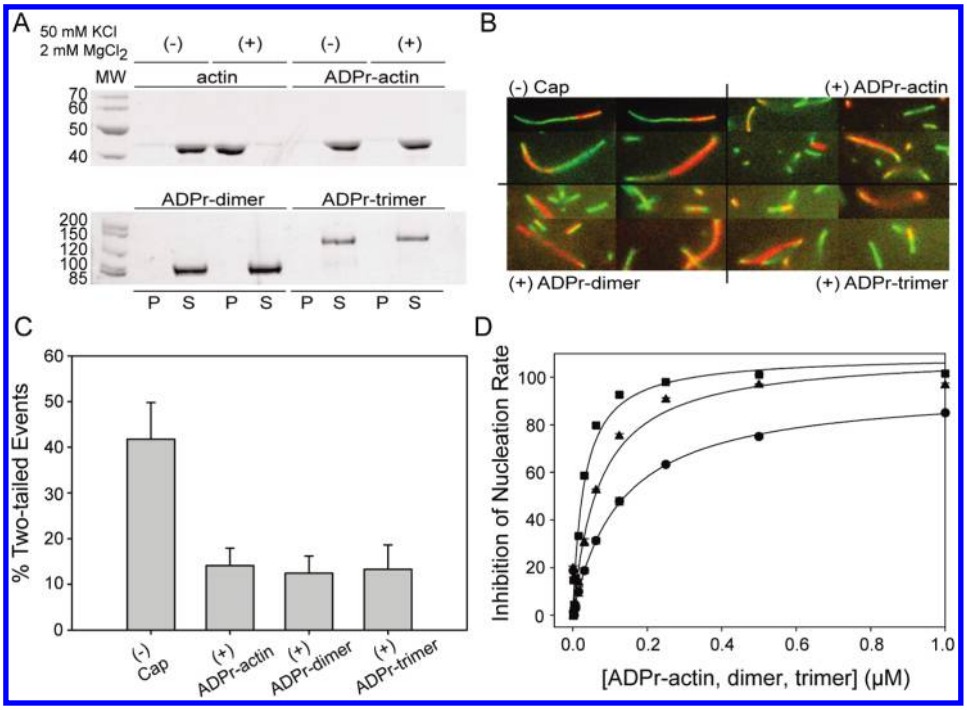

FIGURE 5: ADP-ribosylation renders actin oligomers polymerization-deficient while retaining pointed-end activity. (A) SDS−PAGE analysis of pellet (P) and supernatant (S) fractions resulting from sedimentation of 10 μM [NBD] actin species in the presence and absence of polymerization salts. (B) Fluorescence microscopy images from dual-color filament capping reactions containing 2 μM actin incubated with F-buffer, stabilized with equimolar rhodamine-phalloidin (red), in the presence of no cap (−) or 0.3 μM either ADPr-actin, ADPr dimer, or ADPr trimer. These red filaments act as nuclei from which 0.4 μM G-actin in the presence of Alexa 488-phalloidin (green) can elongate as described in Experimental Procedures. (C) Histogram of the percentage of filaments containing both red and green tails from the experiments described in (B). The proportion of dual-colored filaments decreased by approximately 75% in the presence of ADPr-actin, ADPr dimer, or ADPr trimer. Shown is the average of at least 300 filaments from six images with standard deviation between images given as error bars. (D) Nucleation rate inhibition by ADPr-actin competition. Reactions were initiated by combining 1 μM F-actin and 5% py-actin with 1 volume of 3 μM actin and 5% py-actin, supplemented with increasing concentrations of ADPr-actin (●), ADPr dimer (■), or ADPr trimer (▲). Binding isotherms yielded apparent dissociation constants (K_d^{app}) of 128 ± 30, 30 ± 5, and 72 ± 16 nM for ADPr-actin, ADPr dimer, and ADPr trimer, respectively. Standard error of the ligand binding isotherm is reported.

the stopped-flow device sheared actin filaments and was therefore a convenient method for measuring rapid sheared F-actin-induced filament nucleation. The presence of increasing concentrations of ADPr-actin oligomers resulted in a decrease in filament nucleation rates. This observation is presumably due to the binding of the ADPr-actin species and its subsequent partial inhibition of nucleation.

A protein binding curve was generated by plotting the inhibition of the rate of fluorescence change from 25 to 50 s versus the concentration of ADPr-actin oligomers (Figure 5D). Binding isotherms yielded apparent dissociation constants (K_d^{app}) of 0.129 ± 0.031, 0.030 ± 0.005, and 0.072 ± 0.016 μM for ADPr-actin, dimer, and trimer, respectively. A dissociation constant (also the C_c) of 0.121 μM for actin monomer at the barbed end of actin filaments has been reported for conditions similar to those used here (*31*). The data show that ADP-ribosylation of actin did not affect the interaction between the pointed end of the modified actin and the barbed end of the actin filament. Furthermore, the observed 4-fold increase in capping activity of ADPr dimer compared to ADPr monomer suggests that the increased activity is a result of a concerted effect between the two actin subunits in the ADPr dimer and that capping activity is not simply the result of two independently acting tethered monomers.

The K_d for an actin trimer binding to a filament barbed end has been reported to be 0.072 μM (*21*); comparison with that measured for the ADPr trimer suggests that the ADPr moieties had no significant effect on its affinity for binding to the barbed end of actin filaments and, furthermore, that the actin trimer also possesses an intact pointed-end surface. The trimer showed a 2.5-fold decreased affinity for the filament barbed end compared to the dimer. We sought to shed light on the matter because, theoretically, both species possess the same pointed-end binding surface which interacts with filament barbed ends.

The dissociation constant can be related to Gibb's free energy, ΔG_f of binding, by the equation:

$$K_d = \exp^{-\Delta G_f/RT}$$

Using the determined values of K_d^{app}, we calculated ΔG_f for ADPr-actin and its oligomers using the above equation (Table 1). These data show that a change in ΔG_f of 0.51 eu (entropy units) would be required to account for the observed difference in K_d^{app} between the ADPr dimer and trimer. The term ΔG_f can be described as the sum of the binding energy (ΔG_b) and the entropic energy (ΔG_s) (*6*, *13*). Using our DLS measurements of molecular radius, the entropic costs associated with binding of ADPr dimer and trimer to the actin filament were calculated. The difference in ΔG_s between ADPr dimer and ADPr trimer was 0.43 eu, suggesting that the observed difference in K_d^{app} is accounted for by the additional mass in the trimer and that the ADPr dimer and trimer form similar longitudinal and lateral contacts with the F-actin barbed end (for a detailed explanation refer to Supporting Information). A key point of these observations is that under polymerization conditions capping activity measurements suggest that the actin dimer and trimer form similar pointed-end interfaces that act in a concerted fashion to bind filament barbed ends.

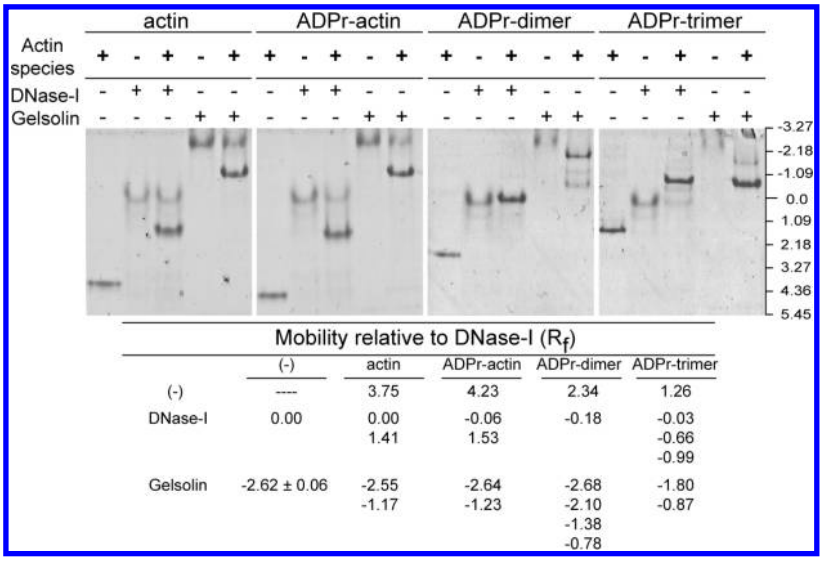

Mobility relative to DNase-I (R_f)

	(-)	actin	ADPr-actin	ADPr-dimer	ADPr-trimer
(-)	----	3.75	4.23	2.34	1.26
DNase-I	0.00	0.00 1.41	-0.06 1.53	-0.18	-0.03 -0.66 -0.99
Gelsolin	-2.62 ± 0.06	-2.55 -1.17	-2.64 -1.23	-2.68 -2.10 -1.38 -0.78	-1.80 -0.87

FIGURE 6: DNase I and gelsolin bind ADP-ribosylated actin complexes. Actin complexes were incubated with a 2-fold molar excess of either DNase I or gelsolin and reaction mixtures analyzed by native PAGE. In the presence of DNase I, predominant bands representative of DNase I−actin complexes are distinguishable for each actin construct. In the presence of gelsolin, actin, ADPr-actin, and its dimer and trimer show the appearance of actin−gelsolin complexes. R_f values were calculated relative to DNase I mobility.

DNase I Binding. DNase I forms a binary complex with actin. The structurally sensitive DNase I binding loop on actin is buried when actin is in filamentous form, and therefore, DNase I binding is restricted to the pointed end of filaments, where the DNase I binding loop remains surface accessible (Supporting Information Figure S3). We utilized DNase I binding as a method for determining the structural compactness of the ADPr dimer and trimer, using native PAGE to visualize binding (Figure 6). Upon treatment with a 2 molar excess of DNase I, all actin species showed the presence of one discrete band, indicative of complex formation. Excess DNase I was observed in the presence of actin or ADPr-actin, since there is only one binding site on actin and the reaction mixture contained a 2 molar excess of DNase I. No excess DNase I was observed in the case of the ADPr dimer, where two potential DNase I binding sites were present, suggesting that both binding sites are amenable to DNase I binding. Since the ADPr trimer possesses the same pointed-end surface as the dimer as well as an additional axial actin, we expected that it would bind at least as much or possibly more DNase I. Interestingly, in the case of ADPr trimer excess DNase I was observed. This implies that the ADPr trimer is able to bind DNase I to a lower extent than ADPr dimer even though it possesses the same pointed-end interface.

The endonuclease activity of DNase I is inhibited upon actin binding; therefore, by monitoring the DNase I activity in the presence of actin complexes, we were able to measure DNase I binding affinities (Figure 7A, Table 2). The affinity of DNase I for actin and ADPr-actin did not change significantly, thus showing that the DNase I binding domain, which is typically considered to be structurally sensitive, is unaffected by ADP-ribosylation at Arg-177. Furthermore, under filament-forming conditions (f-), the DNase I binding affinity for f-ADPr-actin was found to be unaffected.

It is important to note that concentrations and IC_{50} values are reported as [NBD]. To generate stoichiometry values, the following equation was applied:

$$\frac{IC_{50}^{actin}}{IC_{50}^{oligomer}}(n)$$

where n is the number of actin subunits present in the oligomer employed.

DNase I binding affinities for the ADPr dimer and f-ADPr dimer (Figure 7B) were compared to those of the actin monomer. A DNase I:ADPr dimer stoichiometry of 1.96:1 was calculated, correlating with our observations using native PAGE. Increasing the ionic strength resulted in a 2-fold increase in IC_{50}, bringing the DNase I:f-ADPr dimer stoichiometry to 1.07:1. Together, the data imply that f-ADPr dimer is in a state where both actin molecules are accessible to DNase I and that, under high ionic strength, the f-ADPr dimer adopts a closed architecture where only one DNase I binding site is accessible. A binding stoichiometry of 1.34:1 and 1.05:1 was calculated for ADPr trimer and f-ADPr trimer, respectively. These data also corroborate native PAGE observations.

A comparison between ADPr dimer and trimer shows that the third actin molecule does not increase the binding affinity for DNase I but has the opposite effect; it decreases the binding affinity of the oligomer for DNase I. This implies that the presence of the additional actin molecule results in a more structurally compact pointed end. It is possible that the additional lateral and longitudinal contacts formed by the presence of the third cross-linked actin molecule could even induce a twist similar to that seen in the F-actin helix, even under nonpolymerizing conditions. Furthermore, under conditions typically promoting filament formation, both the f-ADPr dimer and f-ADPr trimer are able to bind only one DNase I molecule, suggesting that they can adopt an even tighter conformation. These data validate the idea that both the ADPr dimer and trimer retain a degree of conformational flexibility which could play an important role in ABP binding studies. Furthermore, these results lend credence to our binding affinity calculations which suggested that, under polymerization conditions, the dimer and trimer share the same pointed-end interface.

Gelsolin Binding and Nucleation Rescue. Gelsolin is a well-studied actin filament-severing protein and actin filament nucleator known to simultaneously bind multiple actin molecules (for a review see ref *38*). Native PAGE was used to visualize the binding of gelsolin to actin, ADPr-actin, dimer, and trimer (Figure 6). Native PAGE showed that both actin and ADPr-actin form gelsolin−actin complexes with relative R_f values of

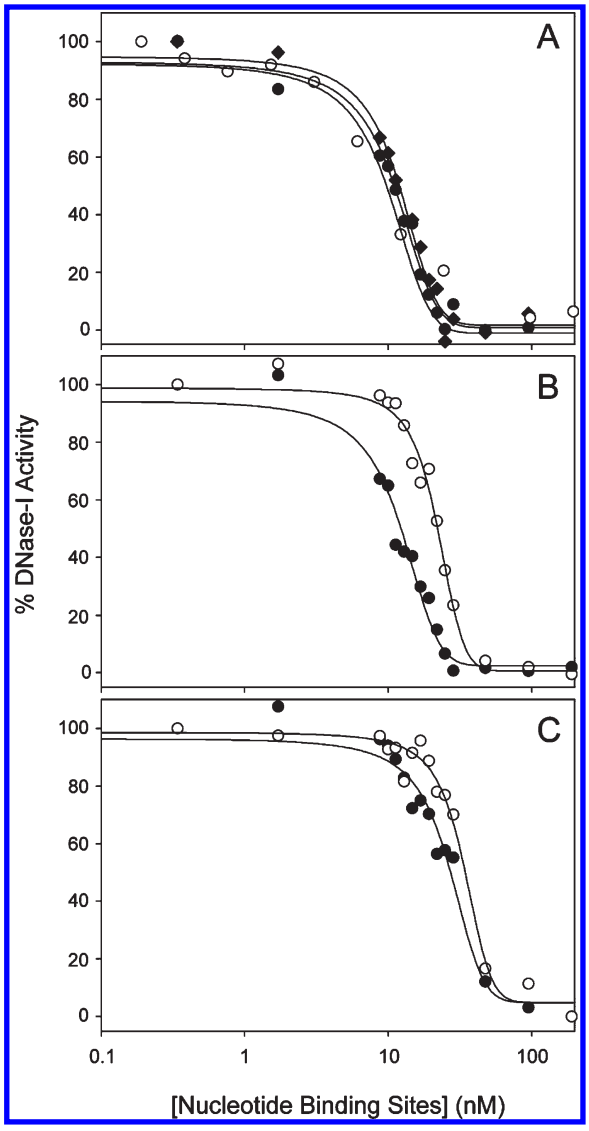

FIGURE 7: DNase I inhibition by ADPr-actin oligomers shows conformational flexibility in low and high ionic strengths. DNase I inhibition by (A) actin (◆), ADPr-actin (●), and ADPr-actin supplemented with 50 mM KCl and 2 mM $MgCl_2$ (f-, ○), (B) ADPr dimer (●) and f-ADPr dimer (○), and (C) ADPr trimer (●) and f-ADPr trimer (○). Both DNase I binding domains on the actin dimer subunits were accessible at low ionic strengths; however, at increased ionic strength, ADPr dimer showed a 2-fold increase in DNase I IC_{50}. At low ionic strength ADPr trimer showed higher protection on a per subunit basis than ADPr dimer, and an increase in ionic strength showed, as with the dimer, increased protection to DNase I.

Table 2: DNase I Inhibition IC_{50} Determinations under Polymerizing (+) and Nonpolymerizing (−) Conditions

	IC_{50} (nM)		binding ratio	
species	−	+	−	+
actin	11.83 ± 0.78			
ADPr-actin	10.98 ± 0.84	9.84 ± 2.37	1.08 ± 0.11	1.20 ± 0.30
ADPr dimer	12.10 ± 0.97	22.08 ± 0.77	1.96 ± 0.15	1.07 ± 0.07
ADPr trimer	26.43 ± 2.08	33.65 ± 1.79	1.34 ± 0.10	1.05 ± 0.07

−1.17 and −1.23 units, respectively. Previously, it has been reported that gelsolin forms a ternary complex with two actins in an antiparallel conformation (*12*), and therefore we believe that the reported R_f values are representative of a gelsolin antiparallel actin ternary complex.

In the presence of gelsolin, ADPr dimer showed a major band at R_f = −2.1 and minor bands at −1.38 and −0.78, where the band at −0.78 appeared to be of equal intensity to that at R_f = −2.1. To shed light on the stoichiometry of the complex formed between ADPr dimer and gelsolin, native PAGE was performed with increasing ratios of gelsolin to ADPr dimer. Interestingly, all protein complex bands appeared simultaneously, and dimer bands disappeared at ratios of gelsolin to actin ≥1 (Supporting Information Figure S6), suggesting a near 1:1 binding ratio of gelsolin to ADPr dimer with at least two different modes of binding. Gelsolin possesses three actin binding domains: two bind monomeric actin, and the third binds only filamentous actin (*33*). It has already been shown that the two monomer binding sites bind actin in an antiparallel conformation (*12*), and it is unlikely that the lateral ADPr dimer would be able to adopt an antiparallel conformation. Therefore, it is possible that the two binding modes are representative of either of the two actin monomer binding sites on gelsolin binding to the dimer.

ADPr trimer binding to gelsolin showed one major band at −0.87 and a minor band at −1.80 (sometimes not observable), also with a binding stoichiometry of 1:1 (Supporting Information Figure S6). The nature of the increase in R_f observed for the gelsolin trimer complex with respect to the gelsolin dimer complex is difficult to ascertain. Both dimer and trimer appear to form 1:1 complexes; therefore, it is unlikely that the lower R_f of the gelsolin dimer complex is due to multiple dimers binding. Native PAGE results are not necessarily representative of molecular weight but are more so representative of shape and charge. The addition of the axial actin in the trimer would result in an increased negative charge. It is possible that the gelsolin trimer complex adopts a more tightly packed conformation than the gelsolin dimer complex. An increase in charge, but not size, explains the increased R_f for the gelsolin trimer complex. As mentioned prior, gelsolin possesses an F-actin binding domain. It is likely that the interface formed by the axially arranged actin subunits in the trimer forms an interface that is able to bind the F-actin binding domain of gelsolin. This would support the notion of a compact gelsolin−trimer complex.

We probed for actin filament nucleation in the presence of the purified ADPr trimer−gelsolin heterocomplex (Figure 8A). Nucleation by gelsolin is believed to occur through two main processes: (1) nucleus formation by binding and coordination of actin molecules and (2) severing of short actin filaments to form nuclei. As calcium is required for gelsolin binding to actin and for the maintenance of gelsolin severing, it can be said that both processes are calcium-dependent. Once bound in a gelsolin−actin complex, calcium is protected from chelation by EGTA, and thus gelsolin nucleation can, in that case, be considered calcium insensitive. We found that gelsolin prebound to actin acted as a strong filament nucleator in the presence of calcium and as a weak nucleator when severing is abolished (no free Ca^{2+}). The ADPr trimer−gelsolin heterocomplex showed significant nucleation activity, suggesting that the binding of gelsolin remodels the ADPr trimer structure to one that is nucleation competent. Furthermore, the nucleation activities of the ADPr trimer are unaltered in the presence or absence of calcium, showing that nucleation rescue is not dependent on severing. It is unlikely that the covalently cross-linked trimer is able to adopt the antiparallel conformation implicated in gelsolin-mediated actin coordination; therefore, we believe that the ADPr trimer−gelsolin complex may be similar to that expected from gelsolin binding to the barbed end of F-actin (*12*, *24*). These results provide an example

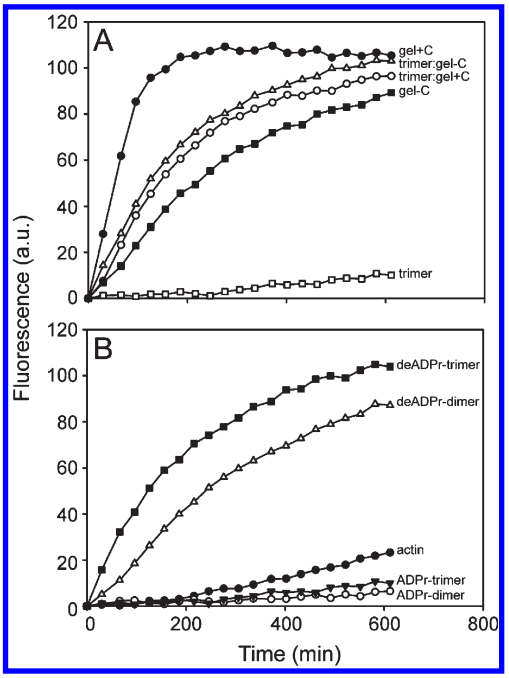

FIGURE 8: Rescue of filament assembly nucleation properties. (A) ADPr trimer lacks actin filament nucleation capabilities (□, trimer). Gelsolin in the presence (●, gel + C) and absence of calcium (▲, gel − C) shows different nucleation capabilities owing to a lack of severing activity in the absence of calcium. ADPr trimer−gelsolin nucleation was also tested in the presence (○, trimer:gel + C) and absence of calcium (Δ, trimer:gel − C) and showed little variance. (B) Actin filament elongation rates (●) in the presence of ADPr dimer (○) or ADPr trimer (▲) lack nucleating activity. After removal of the ADP-ribose moiety from the actin oligomers, the nucleation activity of deADPr dimer (Δ) and deADPr trimer (■) was significantly increased.

of how these actin oligomers may be used to study the structure and function of F-actin binding proteins.

Removal of ADP-Ribose and Nucleation Rescue. The presence of the ADP-ribose on Arg-177 may interfere with the proper binding of ABPs, and therefore the removal of the ADP-ribose moiety may be desirable. Previous reports have described the enzyme-mediated removal of an ADP-ribose moiety from Arg-177 of actin (*15*). In the presence of nicotinamide, the reverse reaction to ADP-ribosylation is favored, and de-ADP-ribosylation is possible, restoring the polymerization properties of actin. Treating the ADPr-actin oligomers with nicotinamide and photox resulted in a rescue of the filament nucleation properties of actin dimers and trimers, with the latter acting as more potent nuclei (Figure 8B). These data suggest that removal of the ADP-ribose moieties from the ADPr-actin oligomers is possible. The degree of control and manageability offered by ADP-ribosylation gives it an advantage over other methods for introducing polymerization deficiencies.

CONCLUSION

In summary, we provide a two-step process for the production of large quantities of polymerization-deficient F-actin oligomers. These oligomers retain their affinity for association with the barbed end of actin and also retain a certain degree of conformation flexibility which is thought to be present in actin filaments. Furthermore, we show that both DNase I and gelsolin are able to bind these actin oligomers, with the latter producing a conformational change responsible for nucleation rescue. We believe that, in the future, the polymerization-deficient F-actin trimer will be able to act as a scaffold for a variety of F-actin-side binding proteins such as myosin. The work presented will form the foundation for research involving the use of F-actin oligomers as an F-actin structural scaffold.

ACKNOWLEDGMENT

We thank Gerry Prentice for early preparations of photox and technical expertise.

SUPPORTING INFORMATION AVAILABLE

A detailed explanation of the theoretical energy requirements of the dimer and trimer and figures showing copolymerization traces of actin and ADPr-actin (S1), cross-linking reaction conditions (S2), structural model of the actin complexes (S3), polymerization traces for the inhibition of nucleation by ADPr-actin species (S4), pyrene fluorescence measurements of ADPr-actins (S5), and binding stoichiometry of gelsolin and ADPr dimer and trimer. This material is available free of charge via the Internet at http://pubs.acs.org.

REFERENCES

1. Ballweber, E., Galla, M., Aktories, K, Yeoh, S., Weeds, A. G., and Mannherz, H. G. (2001) Interaction of ADP-ribosylated actin with actin binding proteins. *FEBS Lett. 508*, 131–135.
2. Chik, J. K., Lindberg, U., and Schutt, C. E. (1996) The structure of an open state of beta-actin at 2.65 Å resolution. *J. Mol. Biol. 263*, 607–623.
3. Cooper, J. A., Walker, S. B., and Pollard, T. D. (1983) Pyrene actin: documentation of the validity of a sensitive assay for actin polymerization. *J. Muscle Res. Cell Motil. 4*, 253–262.
4. Dawson, J. F., Sablin, E. P., Spudich, J. A., and Fletterick, R. J. (2003) Structure of an F-actin trimer disrupted by gelsolin and implications for the mechanism of severing. *J. Biol. Chem. 278*, 1229–1238.
5. dos Remedios, C. G., Chhabra, D, Kekic, M., Dedova, I. V., Tsubakihara, M., Berry, D. A., and Nosworthy, N. J. (2003) Actin binding proteins: regulation of cytoskeletal microfilaments. *Physiol. Rev. 83*, 433–473.
6. Erickson, H. P. (1989) Co-operativity in protein-protein association. The structure and stability of the actin filament. *J. Mol. Biol. 206*, 465–474.
7. Fernandes, M. X., Ortega, A., Lopez Martinez, M. C., and Garcia de la, T. J. (2002) Calculation of hydrodynamic properties of small nucleic acids from their atomic structure. *Nucleic Acids Res. 30*, 1782–1788.
8. Gilbert, H. R., and Frieden, C. (1983) Preparation, purification and properties of a crosslinked trimer of G-actin. *Biochem. Biophys. Res. Commun. 111*, 404–408.
9. Graceffa, P., and Dominguez, R. (2003) Crystal structure of monomeric actin in the ATP state. Structural basis of nucleotide-dependent actin dynamics. *J. Biol. Chem. 278*, 34172–34180.
10. Harris, E. S., Li, F., and Higgs, H. N. (2004) The mouse formin, FRLalpha, slows actin filament barbed end elongation, competes with capping protein, accelerates polymerization from monomers, and severs filaments. *J. Biol. Chem. 279*, 20076–20087.
11. Hegyi, G., Mak, M., Kim, E., Elzinga, M., Muhlrad, A., and Reisler, E. (1998) Intrastrand cross-linked actin between Gln-41 and Cys-374. I. Mapping of sites cross-linked in F-actin by N-(4-azido-2-nitrophenyl) putrescine. *Biochemistry 37*, 17784–17792.
12. Hesterkamp, T, Weeds, A. G., and Mannherz, H. G. (1993) The actin monomers in the ternary gelsolin:2 actin complex are in an antiparallel orientation. *Eur. J. Biochem. 218*, 507–513.
13. Howard, J. (2001) *Mechanics of Motor Proteins and the Cytoskeleton*, Sinauer Associates: Sunderland.
14. Joel, P. B., Fagnant, P. M., and Trybus, K. M. (2004) Expression of a nonpolymerizable actin mutant in Sf9 cells. *Biochemistry 43*, 11554–11559.
15. Just, I., Geipel, U., Wegner, A., and Aktories, K. (1990) De-ADP-ribosylation actin by *Clostridium perfringens* iota-toxin and *Clostridium botulinum* C2 toxin. *Eur. J. Biochem. 192*, 723–727.
16. Kabsch, W., Mannherz, H. G., Suck, D., Pai, E. F., and Holmes, K. C. (1990) Atomic structure of the actin:DNase I complex. *Nature 347*, 37–44.

17. Klenchin, V. A., Khaitlina, S. Y., and Rayment, I. (2006) Crystal structure of polymerization-competent actin. *J. Mol. Biol. 362*, 140–150.
18. Knight, P., and Offer, G. (1978) p-NN′-phenylenebismaleimide, a specific cross-linking agent for F-actin. *Biochem. J. 175*, 1023–1032.
19. Kudryashov, D. S., and Reisler, E. (2003) Solution properties of tetramethylrhodamine-modified G-actin. *Biophys. J. 85*, 2466–2475.
20. Laemmli, U. K. (1970) Cleavage of structural proteins during the assembly of the head of bacteriophage T4. *Nature 227*, 680–685.
21. Lal, A. A., Korn, E. D., and Brenner, S. L. (1984) Rate constants for actin polymerization in ATP determined using cross-linked actin trimers as nuclei. *J. Biol. Chem. 259*, 8794–8800.
22. Mannherz, H. G., Ballweber, E., Hegyi, G., and Goody, R. S. (2008) Cross-linked long-pitch actin dimer forms stoichiometric complexes with gelsolin segment 1 and/or deoxyribonuclease I that nonproductively interact with myosin subfragment 1. *Biochemistry 47*, 9335–9343.
23. Margarit, S. M., Davidson, W., Frego, L., and Stebbins, C. E. (2006) A steric antagonism of actin polymerization by a salmonella virulence protein. *Structure 14*, 1219–1229.
24. McGough, A., Chiu, W., and Way, M. (1998) Determination of the gelsolin binding site on F-actin: implications for severing and capping. *Biophys. J. 74*, 764–772.
25. Mockrin, S. C., and Korn, E. D. (1981) Isolation and characterization of covalently cross-linked actin dimer. *J. Biol. Chem. 256*, 8228–8233.
26. Morrison, S. S., and Dawson, J. F. (2007) A high-throughput assay shows that DNase I binds actin monomers and polymers with similar affinity. *Anal. Biochem. 364*, 159–164.
27. Nair, U. B., Joel, P. B., Wan, Q., Lowey, S., Rould, M. A., and Trybus, K. M. (2008) Crystal structures of monomeric actin bound to cytochalasin D. *J. Mol. Biol. 384*, 848–864.
28. Oda, T., Iwasa, M., Aihara, T., Maeda, Y., and Narita, A. (2009) The nature of the globular- to fibrous-actin transition. *Nature 457*, 441–445.
29. Pengelly, K., Loncar, A., Perieteanu, A. A., and Dawson, J. F. (2009) Cysteine engineering of actin self-assembly interfaces. *Biochem. Cell Biol. 87*, 663–675.
30. Perieteanu, A. A., Sweeting, B., and Dawson, J. F. (2008) The real-time monitoring of the thermal unfolding of tetramethylrhodamine-labeled actin. *Biochemistry 47*, 9688–9696.
31. Pollard, T. D. (1986) Rate constants for the reactions of ATP- and ADP-actin with the ends of actin filaments. *J. Cell Biol. 103*, 2747–2754.
32. Pollard, T. D., and Cooper, J. A. (1986) Actin and actin-binding proteins. A critical evaluation of mechanisms and functions. *Annu. Rev. Biochem. 55*, 987–1035.
33. Pope, B., Way, M., and Weeds, A. G. (1991) Two of the three actin-binding domains of gelsolin bind to the same subdomain of actin. Implications of capping and severing mechanisms. *FEBS Lett. 280*, 70–74.
34. Sawaya, M. R., Kudryashov, D. S., Pashkov, I., Adisetiyo, H., Reisler, E., and Yeates, T. O. (2008) Multiple crystal structures of actin dimers and their implications for interactions in the actin filament. *Acta Crystallogr., Sect. D: Biol. Crystallogr. 64*, 454–465.
35. Schuler, H., Lindberg, U., Schutt, C. E., and Karlsson, R. (2000) Thermal unfolding of G-actin monitored with the DNase I-inhibition assay stabilities of actin isoforms. *Eur. J. Biochem. 267*, 476–486.
36. Sheterline, P., Clayton, J., and Sparrow, J. (1995) Actin. *Protein Profile 2*, 1–103.
37. Spudich, J. A., and Watt, S. (1971) The regulation of rabbit skeletal muscle contraction. I. Biochemical studies of the interaction of the tropomyosin-troponin complex with actin and the proteolytic fragments of myosin. *J. Biol. Chem. 246*, 4866–4871.
38. Sun, H. Q., Yamamoto, M., Mejillano, M., and Yin, H. L. (1999) Gelsolin, a multifunctional actin regulatory protein. *J. Biol. Chem. 274*, 33179–33182.
39. Visschedyk D. D., Perieteanu A. A., Turgeon Z. J., Fieldhouse R. J., Dawson J. F., and Merrill A. R. (2010) Photox: a novel actin-targeting mono-ADP-ribosyltransferase from *Photorhabdus luminescens*. *J. Biol. Chem.*
40. Wegner, A, and Aktories, K. (1988) ADP-ribosylated actin caps the barbed ends of actin filaments. *J. Biol. Chem. 263*, 13739–13742.
41. Wertman, K. F., Drubin, D. G., and Botstein, D. (1992) Systematic mutational analysis of the yeast ACT1 gene. *Genetics 132*, 337–350.